Covalent and Selective Grafting of Polyethylene Glycol Brushes at the Surface of ZIF-8 for the Processing of Membranes for Pervaporation

Marvin Benzaqui, Rocio Semino, Florent Carn, Sérgio Rodrigues Tavares,
Nicolas F Menguy, Mónica Giménez-Marqués, Elena Bellido, Patricia
Horcajada, Thomas Berthelot, Anna Kuzminova, et al.

Covalent and Selective Grafting of PEG Brushes at the Surface of ZIF-8 for the Processing of Membranes for Pervaporation.

Marvin Benzaqui,[‡,‖] Rocio Semino,[ζ,] Florent Carn,[φ] Sergio Rodrigues Tavares,[ζ] Nicolas Menguy,[⊥] Mónica Giménez-Marqués,[‡,‖] Elena Bellido,[‡] Patricia Horcajada,[∂,‡] Thomas Berthelot,[Δ] Anna I. Kuzminova,[§] Maria E. Dmitrenko,[§] Anastasia V. Penkova,[§] Denis Roizard,[#] Christian Serre,[‖,‡,*] Guillaume Maurin,[ζ,*] Nathalie Steunou[‡,*]

[‡]Institut Lavoisier de Versailles, UMR CNRS 8180, Université de Versailles St Quentin en Yvelines, Université Paris Saclay, 45 avenue des Etats-Unis 78035 Versailles Cedex. France. E-mail : nathalie.steunou@uvsq.fr.

[‖]Institut des Matériaux Poreux de Paris, FRE 2000 CNRS, Ecole Normale Supérieure, Ecole Supérieure de Physique et des Chimie Industrielles de Paris, PSL Research University, 75005 Paris, France. E-mail : christian.serre@ens.fr.

[ζ] Institut Charles Gerhardt Montpellier UMR 5253 CNRS, Université de Montpellier, Place E. Bataillon, 34095 Montpellier Cedex 05, France. E-mail : Guillaume.Maurin@univ-montp2.fr.

[φ] Laboratoire Matière et Systèmes Complexes (MSC), UMR CNRS 7057, Université Paris Diderot, Bât. Condorcet, 10 rue A. Domon et L. Duquet, 75013 Paris, France.

[⊥] Sorbonne Université, UMR CNRS 7590, Muséum National d'Histoire Naturelle, IRD, Institut de Minéralogie, de Physique des Matériaux et de Cosmochimie, IMPMC, 75005 Paris, France.

[∂] Advanced Porous Materials Unit, IMDEA Energy, Av. Ramón de la Sagra 3, 28935 Móstoles, Madrid, Spain.

[Δ] SPCSI Chemistry of Surfaces and Interfaces Group, CEA, IRAMIS F-91191, Gif-sur-Yvette, France.

[§] St. Petersburg State University, 7/9 Universitetskaya Nab., St. Petersburg 199034, Russia

[#]Laboratoire Réactions et Génie des Procédés, CNRS, Université de Lorraine, ENSIC, 1 rue Granville, 54000 Nancy, France.

ABSTRACT

The so-called Graftfast reaction in water and at room temperature (RT) was applied to graft polyethylene glycol (PEG) at the surface of the microporous zeolitic imidazolate framework ZIF-8 nanoparticles (NPs) using acrylPEG of different chain lengths (480 Da and 5 kDa). In comparison to non-modified ZIF-8 NPs, both chemical and colloidal stabilities of PEGylated ZIF-8 NPs are significantly enhanced in water. A series of colloidal complex fluids by mixing PEG grafted ZIF-8 (i. e. PEG-g-ZIF-8) NPs with different amounts of polyvinylalcohol (PVA) was prepared and characterized by advanced characterization tools such as dynamic light scattering (DLS) and small-angle X-ray scattering (SAXS) thereby showing their long-term colloidal stability. Finally, dense and supported mixed matrix membranes were cast from PEG-g-ZIF-8/PVA solutions and have shown high performance in isopropanol (IPA) dehydration by pervaporation. The permeation flux of the supported MMM (i. e. 0.091 kg/(m²h) is eleven times higher than that of the pure PVA membrane and these MMMs present a high separation factor (i. e. 7326). These transport properties are presumably due to the molecular sieving effects induced by ZIF-8 and the good interfacial properties of the membrane. The computational exploration of the ZIF-8/PVA and PEG/PVA interfaces provides a microscopic scale explanation for the enhanced compatibility of PVA with the PEGylated MOF when compared to that for the composite based on the bare ZIF-8 as a filler.

Keywords: MOFs, polyvinylalcohol, membranes, surface modification, pervaporation.

■ **INTRODUCTION**

Metal-Organic Frameworks (MOFs) are crystalline hybrid porous materials composed of organic ligands connected to metal containing subunits.[1,2] Most of them exhibit a large and monodisperse porosity with tunable pore sizes and volumes (typically, 0.2-4 cm^3.g^{-1}, S$_{BET}$~300-7000 m^2/g, pore diameter~ 3-60 Å) often exceeding those of other porous solids. Their structural (crystalline structure, pore size and shape) and functional tunability relies on the high diversity of organic

linkers and inorganic building units that can be combined. Over the past few years, these materials have sparked a great interest for several applications such as gas storage/separation, catalysis, sensing, biomedicine etc…[1,2] In order to tune their physico-chemical properties, different strategies[3,4] such as post synthetic modification[5,6] or solvent assisted ligand exchange[7] were proposed to modify the internal surface of MOFs on metal sites or organic linkers. In contrast, the functionalization of the outer surface of MOFs particles remains a challenging objective for numerous nanoscale MOFs while it is of primary importance for their practical use. In biomedicine, the coupling of MOFs nanoparticles with biocompatible polymers (cyclodextrin, chitosan, heparin, poly(ethylene glycol) (PEG)) was first envisaged to enhance their stability in biological environments and improve the pharmacokinetic profile of drugs.[8,9,10,11,12] Despite the success achieved in these pioneer works, one remaining important issue is related to the low or non-controlled amount of polymer, the possible partial accommodation of polymer chains in the porosity of MOFs as well as a lack in the selectivity of the modification process. Since the functional groups may be large enough to access to the porosity, the functionalization of the bulk surface of MOFs may take place together with the surface modification of NPs.

Due to their outstanding gas and liquid separation properties, MOFs NPs were also incorporated as selective porous fillers in polymer matrices to form mixed matrix membranes (MMMs).[13,14,15,16,17] These composite membranes combine the attractive transport and separation properties of the incorporated NPs with the good processability and mechanical properties of the polymers. However, whatever the targeted domain of application (biomedicine, separation…), the MOFs/polymer composites suffer from several limitations mainly related to a low compatibility between MOFs and polymers.[13-16] To cope with these problems, an efficient surface modification of MOFs is required. In general, the most desirable surface modification of MOFs NPs is a selective covalent grafting of a thin organic or polymeric layer at their external surface with a good control of the surface density of functional groups while preserving the crystalline structure and the porosity of the MOF. Indeed, the stability of polymer grafted particles is significantly higher than that of

modified particles with polymer chains physically adsorbed, especially in solution or complex media. Covalent routes were explored taking profit of specific interactions involving externally exposed functional sites present at the surface of MOF NPs such as vacant coordination sites or unsaturated functional groups of the organic linker.[18] Terminal phosphate-modified biomolecules such as cyclodextrins, nucleotides or lipids were covalently attached at the surface of MOFs NPs through metal-phosphate coordination bonds, leading in some cases to a significant improvement of the colloidal stability of MOFs NPs.[19,20,21,22] Another strategy consists of introducing active unsaturated or nucleophilic functions in the organic linker that can be coupled to specific functions of polymers through carbodiimide-mediated amidation or click chemistry.[23,24,25] Furthermore, the robust "grafting from" polymerization technique was used to grow polymer chains from pretethered active sites at the MOFs surface.[26,27] However, such method involves the reactivity of an initiator-carrying linker, thereby leading to the inevitable polymer insertion in the MOF porosity. Except the UV-induced photo-polymerization approach recently reported,[28] most modification methods are not applicable to any MOF structure regardless its surface chemistry. Therefore, there is still an urgent need to develop a general method without any pre-modification or immobilization of initiators. The difficulty is related to the surface chemistry of MOFs which is 'by essence' complex and heterogeneous due to the possible presence of organic and inorganic building units at the surface as well as vacant coordination sites, surface defects and coordinating solvent molecules.[29] A computational approach was thus developed to model MOF surfaces and their interfacial properties with polymers, in order to deepen our understanding of the key parameters that govern the structural characteristics of these systems.[30,31,32]

In this work, we propose a novel and general selective functionalization approach based on the covalent coupling of PEG at the surface of MOF NPs. This synthesis method called Graftfast® was previously developed to covalently graft organic polymer films with controlled thickness onto various surfaces (glass, metal, Teflon, natural plastic, ceramics, NPs…).[33,34] In comparison to other functionalization approaches, Graftfast presents numerous advantages: i) this simple process occurs

4

in a single step and is completed in a short delay of time. ii) this is a highly versatile protocol that can be used to anchor selectively a large number of polymers at the surface of particles, iii) finally, the reactions take place at RT and in water which makes this process biocompatible, sustainable and scalable. Here, this grafting strategy was applied to a topical MOF, i.e. the Zeolitic Imidazolate Framework ZIF-8 (see Figure S1 of SI) which has attracted great attention for a wide range of applications covering the fields of biomedicine, biocatalysis or separations among others.[7,35,36] ZIF-8 has a sodalite topology with pore apertures and diameters of ca. 3.4 Å and 11.6 Å. ZIF-8 has been used to design MMMs for gas separation and pervaporation due to its molecular sieving properties, low cost and easy fabrication.[31,37,38,39] ZIF-8 was perceived as an intrinsically chemically robust material owing to its hydrophobic nature and strong coordination bond between the metal centers and the nitrogen atoms of the imidazolate ligands. However, numerous recent studies have clearly shown that both ZIF-8 crystallites or membranes degrade in aqueous solutions,[40] as a result of a dissolution of ZIF-8 even at RT.[41,42,43,44] In addition, a lack of colloidal stability of ZIF-8 NPs in solvents or polymers has been observed and may lie in the formation of Zn–imidazolate–Zn bonds between particles during the drying, thus resulting in strong adhesive interparticle forces.[31] The strong agglomeration of ZIF-8 particles and their insufficient affinity toward polymer chains can lead to a poor dispersion of MOFs fillers in the polymer matrix, thereby creating interphase defects (macro or nanovoids). Such voids may provide nonselective bypasses through the MMMs that could reduce the separation efficiency and compromise performance. This is one of the main limitations for the processing of composites or defect-free membranes.[13-16] Such scientific hurdles motivated us to apply the Graftfast strategy to this MOF. PEGylated ZIF-8 NPs with PEG chains of two different lengths (480 and 5000 Da) were synthesized and fully characterized by coupling multiple advanced characterization tools (i. e. PXRD, TGA, N_2 porosimetry, DLS, STEM-HAADF). Then, we have explored the compatibility between PEGylated ZIF-8 NPs and PVA by coupling DLS and SAXS experiments. Finally, colloidal solutions of PEG-g-ZIF-8/PVA with PEG chains of 5 kDa which exhibited a very high stability over time were used to cast dense and

supported MMMs with no interfacial defects. These membranes exhibited very good transport properties for the dehydration of IPA by pervaporation. This can be explained by the higher affinity that exists between PVA and PEG compared to that for PVA and ZIF-8 as shown by the microscopic exploration of the interactions using molecular simulations.

■ **RESULTS AND DISCUSSION**

Synthesis and characterizations of ZIF-8 NPs. ZIF-8 NPs were synthesized at reflux conditions in MeOH by reacting the 2-methylimidazole ligand with zinc nitrate as previously reported[45] (see experimental details in SI). As compared to the RT synthesis,[46] performing the synthesis under reflux conditions allows the formation of smaller ZIF-8 NPs around 25±6 nm in diameter (vs. 45 nm for the RT synthesis) as observed by SEM and TEM (Figure S1 of SI). ZIF-8 NPs were further characterized by PXRD, TGA, FTIR and N_2 porosimetry (Figures 1 and S2 of SI) thus indicating the formation of only monodisperse ZIF-8 NPs.
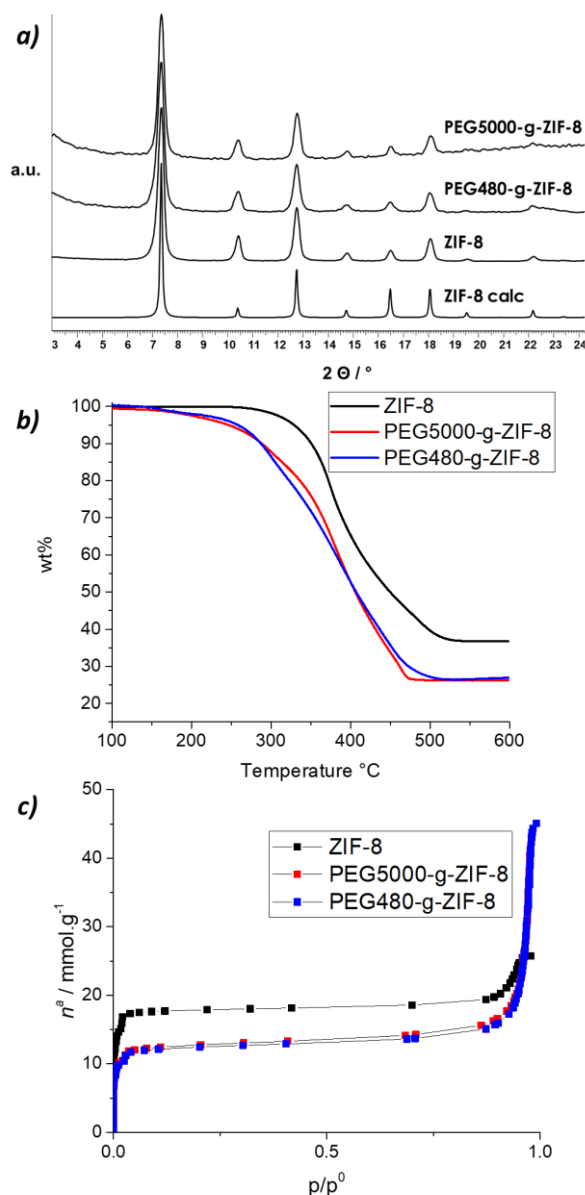
Figure 1. Characterization of ZIF-8 NPs and PEG-g-ZIF-8 NPs with PEG chain lengths of 480 Da and 5 kDa. (a) PXRD, (b) TGA, (c) Nitrogen adsorption isotherms performed at 77 K. Samples were activated at 120 °C for 20 h prior to analysis. PEG-g-ZIF-8 isotherms were normalized with the mass of ZIF-8 (thus excluding the PEG mass).

Grafting PEG brushes at the surface of ZIF-8 NPs. The surface modification of ZIF-8 NPs was performed to enhance their colloidal stability in aqueous solution. PEG was selected owing to its unlimited solubility in water and large excluded volume.[47] Moreover, PEG and PVA are soluble and swollen in water which is a "good solvent" for both polymers.[47] PEG chains of different lengths (480 Da and 5 kDa) were grafted onto ZIF-8 external surface using a diazonium-induced anchoring process (DIAP), also called GraftFast®, described by Palacin *et al*[33,34] and recently applied to MIL-100(Fe) NPs.[48,49] This method involves the chemical reduction in solution of aryldiazonium salt with vinylic groups (see experimental details in SI). First, the chemical reduction of 4 nitrobenzene

7

diazonium salt by cleavage of dinitrogen gives rise to surface-active 4-nitrobenzene radicals. This step is followed by the binding of such radicals to the surface of ZIF-8 through carbon-carbon or/and carbon-metal bonds, as initially reported for other materials.[33,34] The propagation of this reaction, with vinyl functional groups in solution, leads to the formation of an heterogeneous grafted polyphenylene film composed of a mixture of phenylene and vinylic groups at the surface of ZIF-8 NPs. In this work, we thus propose to graft chains of Acryl-PEG onto the external surface of ZIF-8 NPs.
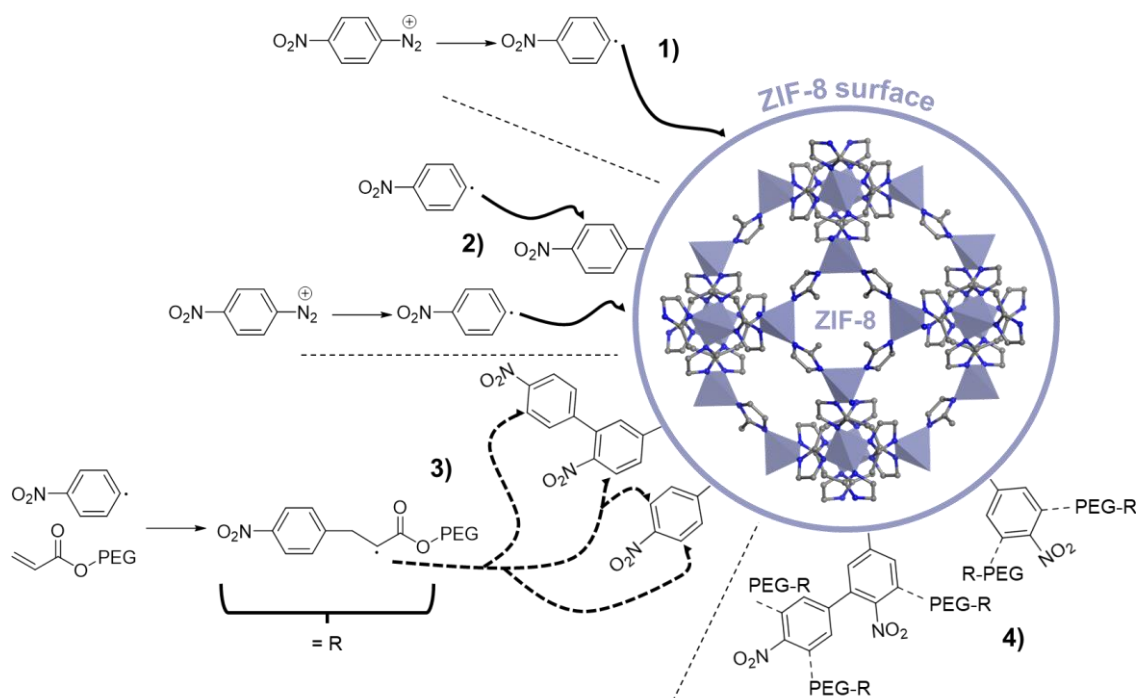
Scheme 1. Simplified scheme representing the supposed grafting mechanism of PEG onto ZIF-8 external surface.

In comparison to previous work reported on MIL-100(Fe) NPs,[48,49] the Graftfast procedure was optimized by using another reducing agent, i.e. ascorbic acid (see experimental details in SI). Here, iron powder is not involved in the modification process of ZIF-8 NPs, thereby avoiding the possible presence of iron or iron oxides impurities in PEGylated ZIF-8 NPs. The scheme 1 depicts the different possible steps of polymer grafting according to the proposed mechanism previously reported.[33,34] 1,2) 4-nitrobenzene diazonium salts are reduced and active radical species are formed followed by their binding to the ZIF-8 surface, giving rise to a grafted nitro-polyphenylene like layer, 3) the radical species can react with the terminal acryl function of PEG to form macro-radical

chains that can react with the nitro-polyphenylene primer layer on ZIF-8 surface, finally 4) additional PEG radicals can interact with the ZIF-8 outer surface, thereby forming a PEG coating at the surface of the NPs. A dark red powder was obtained and the so-called PEG-g-ZIF-8 NPs were further characterized by several techniques to determine the content of PEG and evaluate the crystallinity and porosity of ZIF-8 NPs. The red color suggests that the acryl-PEG moiety is covalently conjugated with the nitro-polyphenylene thin film on ZIF-8 surface. Figure 1(a) shows the PXRD of PEG-g-ZIF-8 NPs with 480 Da and 5 kDa PEG chains. No additional peaks or loss of crystallinity is observed confirming the stability of ZIF-8 NPs upon the grafting process. Thermogravimetric analyses (TGA) were used to evaluate the amount of PEG (wt%) grafted onto ZIF-8 surface (Figure 1(b)). While ZIF-8 NPs are thermally stable up to 300°C, PEG-g-ZIF-8 NPs present an earlier degradation step around 150 °C which may be imparted to the degradation of PEG.[50,51] For both 480 Da and 5 kDa PEG lengths, the amount of PEG in the composite is estimated to 10 wt%, according to the residual amount of oxide at T > 500 °C. TEM images of PEG-g-ZIF-8 NPs show spheroidal NPs with a diameter distribution close to 25 nm in agreement with the pristine non modified ZIF-8 NPs (see Figure S1 of SI).

By assuming ZIF-8 NPs as perfect spheres with smooth surfaces, one can calculate the surface PEG density ($[\Gamma]$), the number of PEG chains per 100 nm^2. This value is close to 53 and 5.2 PEG chains per 100 nm² for 480 Da and 5 kDa PEG lengths, respectively (detailed calculations are available in SI). The lower PEG density with 5 kDa chains may be imparted by the steric hindrance of longer chains at the surface of the particles. This surface PEG density was compared to the theoretical value ($[\Gamma^*]$) required for full surface PEG coverage, assuming that PEG chains are in the mushroom conformation regime.[52,53] At low surface coverage, PEG chains behave as isolated coils and present a conformation called the mushroom regime. With increasing the density of PEG chains, excluded volume interactions between chains take place, thereby forcing PEG chains to extend from the surface and leading to an increase of the layer thickness. $[\Gamma^*]$ thus corresponds to the number of unconstrained PEG molecules per 100 nm^2. As reported previously,[52,53] the $[\Gamma]/[\Gamma^*]$

is indicative of how densely the PEG molecules are packed at the surface of NPs: a ratio<1 indicates a low density of PEG molecules with a mushroom configuration while a ratio >2 indicates a high density of PEG molecules in a dense brush conformation. For both PEG$_{5000}$-g-ZIF-8 and PEG$_{480}$-g-ZIF-8, $[\Gamma]/[\Gamma^*]\sim1.2$, showing that the PEG molecules are in a low-density brush conformation as previously reported for PEGylated MIL-88A or MIL-100(Fe)NPs.[11,48,49]

FT-IR spectra were also recorded (see Figure S2) to further confirm the presence of PEG in the modified ZIF-8 NPs. Besides structural vibration bands of ZIF-8, IR spectra of both PEG-g-ZIF-8 NPs present two sets of additional peaks: {1725, 1260, 1110, 854 cm^{-1}} and {1525, 1340 cm^{-1}} that can be attributed respectively to PEG and nitrobenzene as depicted in Table S1. The low intensity peak at 1728 cm^{-1} corresponds to the carbonyl group of the ester function of the Acryl-PEG. Such specific carbonyl peak is clearly attributed to the polymer contribution since no carbonyl groups are present in the MOF framework. Finally, the selective external surface grafting was assessed by adsorption of N$_2$ at 77 K (see Figure 1(c)). The BET surface area of PEG-g-ZIF-8 NPs and pure ZIF-8 is 1200 m².g^{-1} and 1700 m^2.g^{-1} respectively. The high BET surface area of PEG-g-ZIF-8 NPs indicates that the grafting of ZIF-8 mostly occurs at the external surface of ZIF-8 NPs. The decrease of the BET area upon PEG modification may be explained by the steric hindrance of the PEG chains at the surface of ZIF-8 NPs which limits the accessibility of N$_2$ to the microporous cages of the MOF. The partial accommodation of PEG chains in the porosity of ZIF-8 is not likely to occur, the pore aperture of ZIF-8 (3.4 Å) being significantly lower than the surface area occupied by one PEG molecule (i. e. 22.7 and 2.2 nm^2 for PEG chains of 5000 and 480 Da respectively, see SI for details). Moreover, the pore size distribution of both pristine ZIF-8 and PEGylated ZIF-8 NPs is similar and fully consistent with that reported for ZIF-8 materials (Figure S3 of SI).[54] This is in agreement with the location of PEG chains at the external surface of modified ZIF-8 NPs.

Colloidal stability of PEG-g-ZIF-8 NPs in water and PVA. In order to investigate the impact of PEG on the colloidal stability of ZIF-8 NPs, concentrated solutions of PEG-g-ZIF-8 NPs at 1 g L^{-1}

were prepared in water since they are prone to mimic the real casting solutions used for the processing of ZIF-8/PVA MMMs. For pure ZIF-8 NPs, a strong aggregation process took place since particles with $D_h > 1000$ nm were detected by DLS (Figure S4). With both lengths of PEG chains, a significant decrease of the hydrodynamic diameter was observed in comparison to pure ZIF-8 NPs. Since the particle diameters of PEG_{480}-g-ZIF-8 (i.e. 80 nm) and PEG_{5000}-g-ZIF-8 (i.e. 110 nm) are higher than that of the individual ZIF-8 NPs (Figure S1), it means that the clustering of PEGylated ZIF-8 NPS in pure water is not completely suppressed. However, PEG-gZIF-8 colloids present an enhanced stability in water over time (see Figure S5 of SI for details) which is crucial for the preparation of homogeneous MMMs. These results showed that the PEG surface modification exerts an efficient shielding effect on the dispersion of ZIF-8 NPs through steric repulsions between polymer chains. Actually, it is well known that macromolecular brushes are effective in stabilizing colloidal suspensions.[55] Moreover, upon ageing for about 15 days, PEGylated ZIF-8 NPs present an excellent chemical stability in water, as shown by STEM-HAADF (Figure S6(c) of SI). In contrast, a significant degradation of non-modified ZIF-8 NPs is revealed by STEM-HAADF, showing the presence of micrometer-sized particles with a different morphology (Figure S6(a)). Chemical analyses recorded using a X-ray energy dispersive spectrometer (Figure S6(b)) show that these particles may correspond to zinc hydroxide. As previously reported, ZIF-8 with the sodalite topology is one of structural polymorphs obtained by reacting Zn^{2+} and methylimidazolate building units in water. ZIF-8 is presumably a kinetic polymorph while non-porous Zn-imidazolate or $Zn(OH)_2$ are the thermodynamically stable phases.[36] This suggests that this degradation phenomenon proceeds through a redissolution-crystallization mechanism. Such observations are fully consistent the hydrolysis process of ZIF-8 particles and membranes previously reported.[41-43] Such results clearly show the positive impact of the PEG shell in the stability of ZIF-8 NPs in aqueous solution which is of high interest for the practical use of ZIF-8 NPs in different applications.

We then prepared complex fluids by dispersing PEGylated ZIF-8 NPs in PVA for different PEG-g-ZIF-8/PVA weight ratio and a PEG-g-ZIF-8 concentration of 1 g.L^{-1}. The assembly process of PEG-g-ZIF-8 NPs and PVA was first studied by DLS (Figure S7). The addition of PVA significantly improves the dispersion of pure ZIF-8 NPs in solution, as shown by the strong decrease of the hydrodynamic diameter of the particles. It shows that PVA chains exert also a shielding effect on the dispersion of ZIF-8 NPs. In contrast, the hydrodynamic diameter of PEG-g-ZIF-8 particles was almost constant whatever the PVA amount with values around 100-150 nm from 0 to 70 wt% of PVA and with a maximum at 360 nm for the highest content of PVA (90 wt%). These results show that ZIF-8 NPs are shielded by the PEG molecules that act as the steric barrier for the incoming polymers. Complementary SAXS experiments were conducted on these PEG-g-ZIF-8/PVA solutions in order to clarify the contribution of the NPs assembly to the light scattering. Indeed, DLS can determine the size distribution profile of any kind of particles including inorganic and polymer NPs. In contrast, the SAXS signal is dominated by the scattering of ZIF-8 NPs due to the high mass of MOF and the signal of PVA or PEG is thus negligible. SAXS is thus an accurate tool to evaluate the dispersion of NPs in a complex colloidal solution. SAXS measurements were also performed on diluted colloidal solutions at 0.1 g L^{-1}. Figure 2 shows the evolution of the gyration radius (R_G) for ZIF-8/PVA and PEG-g-ZIF-8/PVA solutions while the SAXS curves are provided in Figure S8. The colloidal solution of pure ZIF-8 NPs presents a low stability at 0.1 g.L^{-1}, as previously reported.[31] In contrast, the R_G value of PEG-g-ZIF-8 NPs is almost constant whatever the PVA amount. By increasing the ZIF-8 concentration to 1 g L^{-1}, one can notice a remarkable colloidal stability of ZIF-8 and PEG-g-ZIF-8 NPs in PVA, as shown by a stable value of R_G whatever the PVA content. It is worth noting that the gyration radius of pure ZIF-8 NPs is significantly higher than that of PEG-g-ZIF-8 NPs, showing the stabilizing effect of the PEG shell on the dispersion of ZIF-8 NPs in PVA. More importantly, the compatibility between PEGylated ZIF-8 NPs and PVA appears more efficient for PEG with longer chain length (i. e. 5 kDa), as indicated by the lower value of R_G (i. e. R_G = 72 nm for PEG$_{480}$-g-ZIF-8 NPs and R_G = 58

12

nm for PEG$_{5000}$-g-ZIF-8). Such observation is in full agreement with a previously reported study on the compatibility of grafted silica particles with poly(methyl methacrylate) matrix.[55] The improved dispersion of particle brushes within the PVA matrix with increasing the degree of polymerization of grafted PEG chains follows the predicted trend proposed by Leibler.[56]
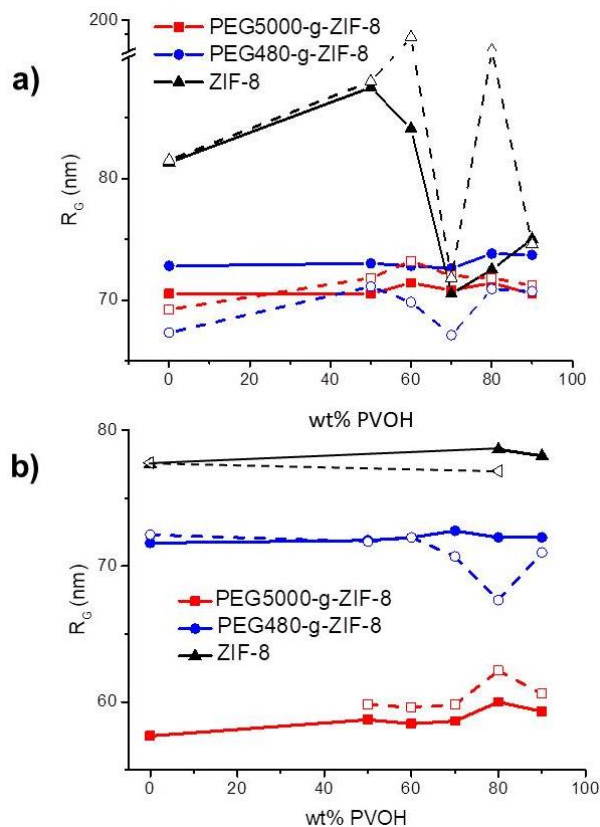
Figure 2. Evolution of the gyration radius (measured by SAXS by Guinier fitting at very small scattering angle) for ZIF-8/PVA solutions at (a) 0.1 g.L^{-1} and (b) 1 g.L^{-1} as a function of PVA content. Empty symbols correspond to the analysis after 24h.

The colloidal stability of these solutions (1 g.L^{-1}) was also evaluated by visual observations over a long period (see Figure S5). While phase separation starts after 30 h for non-modified ZIF-8 NPs, PEG-g-ZIF-8/PVA suspensions are much more stable in time. No phase separation was even observed for PEG$_{5000}$-g-ZIF-8 whatever the amount of PVA for at least one week. Such exceptional long-term colloidal stability is the result of a modified interface between ZIF-8 and PVA chains due to the PEG coating. This is of high interest for the processing of membranes by solvent casting since the sedimentation of particles during the evaporation of the solvent could be avoided. To confirm this result, SAXS data of ZIF-8 and PEG-g-ZIF-8 NPs were collected after 24 h. Only R$_G$

13

increases to some extent for non-modified ZIF-8 NPs at 0.1 g. L^{-1}. For other particles, the intensity of the SAXS signal (and thus R_G) did not change significantly, thereby showing a good colloidal stability of these solutions in this time scale (see Figure 2). PEG$_{5000}$-g-ZIF-8 NPs was finally selected for the processing of membranes due to its excellent dispersion and colloidal stability in PVA solutions.

Preparation and optimization of supported PEG$_{5000}$-g-ZIF-8/PVA membranes for the dehydration of isopropanol (IPA) by pervaporation. IPA is extensively used in semiconductor and pharmaceutical industries. However, its current production involves an energy-intensive azeotropic distillation process and it is of high interest to replace it by low-energy demanding process such as membrane-based dehydration unit.[57] PEG-g-ZIF-8/PVA membranes were thus elaborated for the separation of IPA-H$_2$O mixture by pervaporation. However, as shown by STEM-HAADF, composite films of PEG$_{5000}$-g-ZIF-8/PVA that were cast directly from PEG-g-ZIF-8/PVA suspensions, consist of aggregates with a diameter of a few hundred nanometers (Figure S9 of SI). Note that the drying of solutions on the carbon grids can also induce the aggregation of particles. These preliminary experiments have shown that the dispersion of PEG$_{5000}$-g-ZIF-8 NPs in PVA should be optimized for the processing of high performance MMMs. For that purpose, a reticulation of the MMMs was performed by using glutaraldehyde (GA). It is worth noting that PVA was extensively studied for pervaporation dehydration due to its strong hydrophilicity, excellent chemical stability and good film-forming properties.[58] However, the high swelling of PVA in aqueous solutions is detrimental to the water permselectivity of membranes.[58,59] Therefore, it was reported that this swollen effect could be limited by introducing a cross-linking agent such as GA or by blending the polymer with organic or inorganic fillers.[58,59] Here, GA and PEG-g-ZIF-8 NPs were both introduced into the PVA solution to modify the microstructure of PVA based membrane (interactions between polymer chains and distribution of PEG-g-ZIF-8 NPs) through a synergism effect.

Dense and cross-linked CL-PEG$_{5000}$-g-ZIF-8/PVA membranes with different PEG$_{5000}$-g-ZIF-8 loadings (5, 10 and 15 wt%) were first prepared by solvent evaporation and by using GA as a cross-linking agent (see Figure 3(b) and S10 of SI). Equivalent dense PEG$_{5000}$-g-ZIF-8/PVA MMMs were prepared without GA for comparison (Figure 3(a) and S10). The thickness of the membranes is close to 40 μm. PXRD of CL-PEG$_{5000}$-g-ZIF-8/PVA MMMs (Figure S11) display the XRD peaks of ZIF-8 NP, confirming that the crystalline structure of ZIF-8 is preserved upon the processing of MMMs. Additional XRD peaks are also present on the pattern of MMMs that can be ascribed to PVA due to its semi-crystalline nature as previously reported.[60,61] Cross-sectional SEM images (Figures S12(e,f)) of cross-linked MMMs show the excellent dispersion of PEG$_{5000}$-g-ZIF-8 with the absence of any significant aggregation. In contrast, the agglomeration of PEG$_{5000}$-g-ZIF-8 is more pronounced for non-reticulated PEG$_{5000}$-g-ZIF-8/PVA membranes (Figures S12(b-d)), thereby showing the positive effect of GA on the distribution of the MOF particles. Water contact angles of the CL-PEG$_{5000}$-g-ZIF-8/PVA were measured to evaluate the impact of co-reticulation by the MOF and GA on the hydrophilic properties of PVA. For pure PVA membrane, the value of the contact angle (70°) is about the same for reticulated and non-reticulated membranes. For MMMs, a significant increase of the contact angle is observed by increasing the MOF content (see Table S2 of SI), which is fully consistent with the hydrophobic character of the MOF.

The transport properties of the CL-PEG$_{5000}$-g-ZIF-8/PVA MMMs were studied for the separation of the azeotropic IPA/H$_2$O (88:12 w/w) mixture by pervaporation. Equivalent experiments were performed on the pure PVA or PEG$_{5000}$-g-ZIF-8/PVA membranes for comparison. Cross-linked MMMs based on non-modified ZIF-8 NPs and PVA (i. e. CL-ZIF-8/PVA) were also tested. The separation performance was determined in terms of permeation flux and the IPA/H$_2$O separation factor. It is worth noting that all pure PVA and composite membranes exhibit a remarkable separation factor of about 7326 (water content in the permeate of 99.9 wt%). As shown in Figure 3(d), the permeation flux of both reticulated and non-reticulated MMMs increased significantly with the increase of the ZIF-8 content in the PVA matrix. However, CL-

PEG$_{5000}$-g-ZIF-8/PVA MMMs present higher permeation flux than PEG$_{5000}$-g-ZIF-8/PVA. The best transport properties are observed for the CL-PEG$_{5000}$-g-ZIF-8/PVA membranes with 15 wt% of MOF. Its permeation flux is ~4.7 times higher than that of the pure non-reticulated PVA membrane and ~1.4 times higher than of the PEG$_{5000}$-g-ZIF-8/PVA membrane with the same MOF content. CL-ZIF-8/PVA MMM was also evaluated for IPA/H$_2$O pervaporation, showing a poor performance. The permeation flux values measured on analogous CL-ZIF-8/PVA MMMs are not reproducible and this is fully consistent with a possible degradation of ZIF-8 NPs in the PVA matrix as previously shown (see Figure S6 of SI). In order to enhance the permeability of these membranes, supported MMMs were prepared through the deposition of a thin selective layer of CL-PEG$_{5000}$-g-ZIF-8/PVA (15 wt% MOF) onto a porous polysulfonamide UPM-20 support (see Figure 3(c) and experimental details in SI). As shown by SEM (Figure S13), the thickness of the active layer is 1.5 ± 0.3 µm. This significant decrease of the membrane thickness impacts clearly the transport properties of the MMMs. As shown in Figure 3(e), the permeation flux of the supported CL-PEG$_{5000}$-g-ZIF-8/PVA (15 wt% MOF) MMM is eleven times higher than that of the pure PVA membrane and three times higher than dense CL-PEG$_{5000}$-g-ZIF-8/PVA (15 wt% MOF). It is worth noting that such supported membranes present a high separation factor value of 7326 (water content in the permeate of 99.9 wt%), as previously found for dense CL-PEG$_{5000}$-g-ZIF-8/PVA. Pervaporation experiments were conducted on the CL-PEG$_{5000}$-g-ZIF-8/PVA (15 wt% MOF) membrane for the separation of IPA/H$_2$O (88:12 w/w) mixture during 1 week (see Figure 3(f) and SI). A small variation of the permeation flux of the membrane from 0.091 to 0.12 kg/(m^{2}h) was observed while the water content in the permeate evolved slightly from 99.9 to 98.1 wt.%.These experiments have clearly shown that the separation performance of CL-PEG$_{5000}$-g-ZIF-8/PVA (15 wt% MOF) membrane (i e. permeation flux and selectivity) is stable after continuous PV experiments for 7 days.

The increase of the permeation flux of the membranes by increasing the amount of ZIF-8 with no reduction of the selectivity is in agreement with the absence of any interfacial defects. Such voids at

16

the origin of nonselective bypasses are generally observed in poorly performing MMMs that are characterized by a strong aggregation of MOFs NPs.[14] In contrast, the co-reticulation of PVA with both GA and PEG_{5000}-g-ZIF-8 has produced homogeneous and defect free CL-PEG_{5000}-g-ZIF-8/PVA membranes with a high performance for pervaporation. The functionalization of the membrane by GA significantly enhances the dispersion of PEGylated ZIF-8 NPs in the PVA matrix, as shown by SEM images (Figure S12). The increased permeability should be mainly due to the highly porous character of ZIF-8 while the high separation factor may result from the combined effects of the molecular sieving properties of ZIF-8 and the low degree of swelling of the membrane. ZIF-8 is particularly suitable for the IPA/H_2O separation since its pore aperture diameter of 0.34 nm is between the kinetic diameters of water (0.30 nm) and IPA (0.47 nm). Moreover, as shown in Table S3, the swelling degree of both CL-PEG_{5000}-g-ZIF-8/PVA and PEG_{5000}-g-ZIF-8/PVA membranes is quite low and decreases with the MOF content.

17
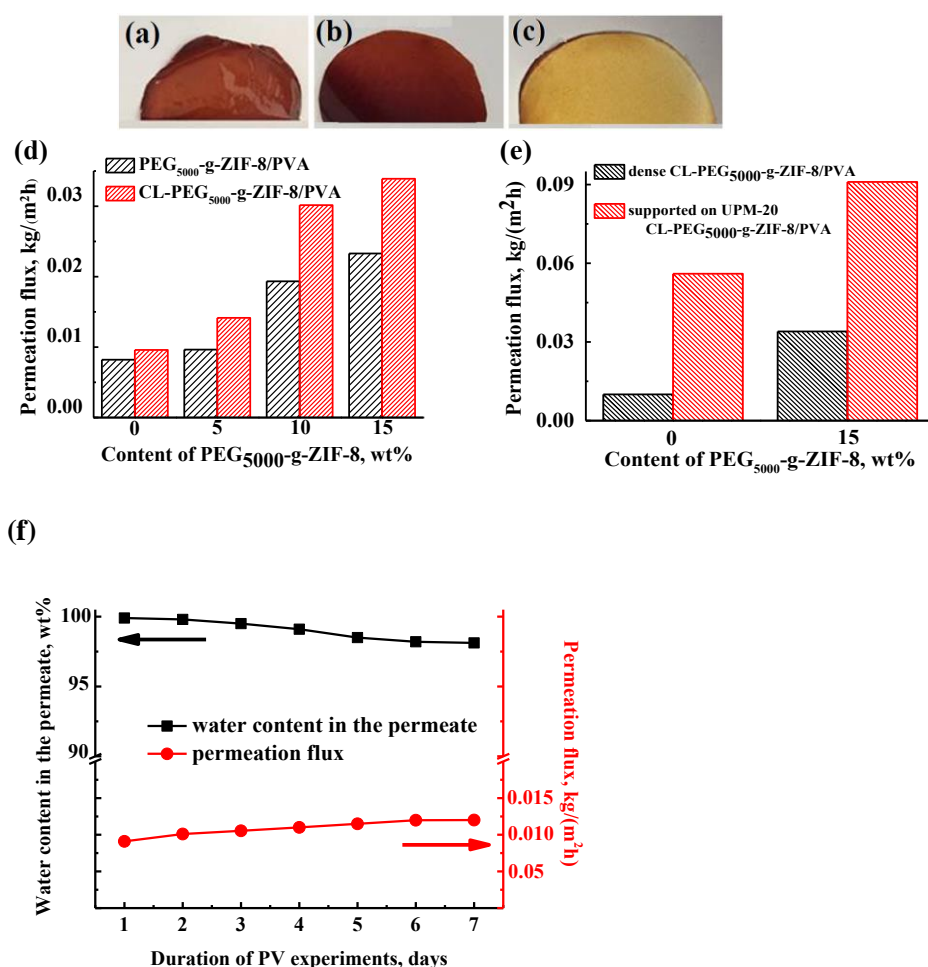
Figure 3. (a-c) Photographs of MMMs with 15 wt% of PEG_{5000}-g-ZIF-8: (a) PEG_{5000}-g-ZIF-8/PVA, (b) CL-PEG_{5000}-g-ZIF-8/PVA, (c) supported CL-PEG_{5000}-g-ZIF-8/PVA;(d,e) permeation flux of membranes as a function of PEG_{5000}-g-ZIF-8 for the pervaporation of the iPrOH (88 wt.%) - water (12 wt.%) mixture at 25°C; (d) comparison of the membrane flux between CL-PEG_{5000}-g-ZIF-8/PVA and PEG_{5000}-g-ZIF-8/PVA membranes; (e) comparison of the membrane flux between dense and supported CL-PEG_{5000}-g-ZIF-8/PVA membranes. (f) Water content in permeate and permeation flux of CL-PEG_{5000}-g-ZIF-8/PVA (15 wt %) for 7 days. The mean accuracy for the transport parameters was as follows: ±5% for permeation flux for dense membranes and ±9% for permeation flux for supported membranes.

Finally, the performance of the supported CL-PEG_{5000}-g-ZIF-8/PVA membrane was compared to that of PVA based MMMs previously reported in literature that were studied under similar conditions for IPA pervaporation dehydration (see Table S4 of SI). However, we need to keep in mind that such comparison of membranes performance should be taken with caution since the results are strongly dependent on the experimental conditions and the microstructure of membranes (thickness). It was observed that the PVA membrane modified by 10 wt% clinoptilolite had the best transport properties (the highest separation factor of 12848 and permeation flux of 0.222 kg/(m^2 h))[62] for the pervaporation dehydration of IPA (10 wt% water) compared to all others hybrid membranes. However, only a dense 10 wt% clinoptilolite/PVA membrane with a 50 μm thickness was prepared due to the diameter of the clay particles (i. e. 2 μm). This strongly limits the practical application of such membrane. In contrast, by using PEGylated ZIF-8 NPs, it was possible to design supported CL-PEG_{5000}-g-ZIF-8/PVA membrane that combines a very high constant separation factor (7326) for pervaporation of IPA-water (12 wt%) mixture and a permeation flux which is comparable or even higher than numerous MMMs previously reported. The lower permeation flux of CL-PEG_{5000}-g-ZIF-8/PVA in comparison to membranes with fillers such as MWNTs-PSS[63] or Clay (clinoptilolite) (10 wt%)[62] is presumably due to the higher crystallinity of the PVA matrix as a result of the cross-linking with PEG_{5000}-g-ZIF-8 (see Figure S11). However, as stated before, the introduction of PEG_{5000}-g-ZIF-8 in the PVA membrane leads to a remarkable increase of the permeation flux in comparison to unmodified PVA-based membrane (see Figure 3). It is worth noting that non modified ZIF-8 NPs were previously combined to PVA for the IPA/H_2O separation by pervaporation.[64] However, this study clearly showed that the introduction of ZIF-8 NPs with a

MOF content as low as 10 wt% led to an increase of the permeability, but at the expense of the separation factor. This drastic reduction of the selectivity was attributed to the aggregation of ZIF-8 NPs in PVA. Finally, similar pervaporation experiments for the separation of H_2O-IPA (12/88 wt%) mixture at 25 °C were conducted on the commercial membrane PERVAP^{TM} 1201 (SULZER) which is classically used for IPA dehydration. It was found that PERVAP^{TM} 1201 membrane presented a permeation flux of 0.016 kg/(m^{2}h) and 99.9 wt% water in the permeate. Therefore, the permeation flux of this commercial membrane is ~6 times lower than that of the supported CL-PEG$_{5000}$-g-ZIF-8/PVA (15 wt% MOF) membrane. These results confirm the high performance of the CL-PEG$_{5000}$-g-ZIF-8/PVA membrane which is certainly in line with the compatibility between the different components in play.

Molecular Modeling of ZIF-8/PEG/PVA and ZIF-8/PVA interfacial structures.

The interfacial properties of the ZIF-8/PEG/PVA membranes were further analyzed by molecular modelling in order to provide a molecular-scale explanation of the good compatibility between the PEGylated ZIF-8 particles and PVA. To start our analysis, we have considered the ZIF-8/PVA interface. The PVA and ZIF-8 atomic density profiles of the corresponding composite are plotted in Figure S17(a). The atomic density of PVA drops almost linearly in the proximity of the {011} ZIF-8 surface, the total width of this region is of (9.0 $\pm$ 0.5) Å. Further away from the MOF, the atomic density of the polymer oscillates. We refer to these regions as *A* and *B* respectively. We can observe that PVA and ZIF-8 coexist in the entire length of *region A*. This means that the polymer adapts very well to the morphology offered by the MOF, the decay of the atomic density of the polymer being due to steric hindrance and not because of a low MOF/polymer affinity. No interfacial microvoids are detected at the ZIF-8/PVA interface, and PVA can even penetrate into the open pores of the ZIF-8 surface. The length of penetration, defined as the total superimposition of MOF and polymer in the *z* coordinate, is of (9.0 $\pm$ 0.4) Å. The main interactions that hold the two components together come from the -OH groups of the polymer with both the -NH and -OH

functions in the ZIF-8 surface, with characteristic average distances of 2.8 Å and 2.7 Å respectively, as shown in the corresponding radial distribution functions plotted in Figures S17(b) and S17(c). Overall, this microscopic picture shows a much higher MOF/polymer contact surface compared to that found for the ZIF-8/PIMs cases,[30,31] which can account for the better MOF/polymer compatibility observed here. This scenario is similar to that of other MOF/polymer systems, such as UiO-66/PEG, UiO-66/PVDF[32] and HKUST-1/PVA.[65] Here, the high degree of compatibility between ZIF-8 and PVA is favoured by the high flexibility of the polymer as previously reported.[32] Illustrations of the –OH(PVA)-OH(ZIF-8) and –OH (PVA)/-NH (ZIF-8) interactions obtained using a cluster-based DFT approach are shown in Figures S18(a) and S18(b). These DFT-optimized geometries are consistent with those obtained from the MD simulations, since they involve interacting distances that are included in the range of values covered by the peaks present in the radial distribution functions plots reported in Figure S17. The DFT-calculated binding energies considering both scenarios are similar, i.e. -30.6 kJ mol^{-1} and -35.3 kJ mol^{-1}, respectively. This emphasizes that the strength of interactions between the PVA and both –NH and –OH functions is very similar and the resulting moderate energy range is compatible with a relatively weak van der Waals interaction.

We have further analyzed the ZIF-8/PEG/PVA case. Since the PEG chains adopt a brush conformation, the ZIF-8/PEG/PVA ternary system can reasonably be treated as a binary PEG/PVA interface. PEG and PVA exhibit characteristic interacting distances of approximately 2.9 Å between (i) the –OH group of PVA and the oxygen atom of PEG and (ii) the hydrogen atoms that belong to the chains of both polymers (Figure 4(a) and 4(b)). These favourable interactions between PVA and PEG provide a driving force towards the mixing of PEG-g-ZIF-8 brushes and PVA. Figure 4 further illustrates the distribution of PEG and PVA in the composite system. One can clearly observe an interpenetration of the polymers which supports their high compatibility. This interpenetration is of (14 ± 2) Å, suggesting a higher contact surface for PEG/PVA than for ZIF-8/PVA where the interpenetration length was of (9.0 ± 0.4) Å. The penetration of the PEG brush by the PVA matrix is

expected to facilitate a uniform dispersion of PEGylated particles in the PVA matrix. This microscopic picture explains the better compatibility that was observed experimentally between PVA and the PEGylated NPs as compared with PVA and the pristine ZIF-8 NPs.
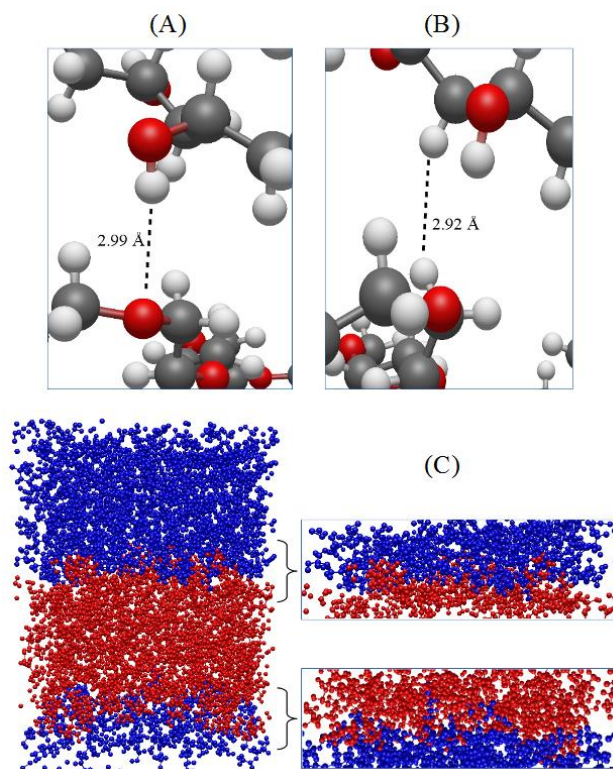
Figure 4. Illustration of the main interactions between PEG and PVA, (A) –OH (PVA) and O (PEG) and (B) –CH (PVA) and –CH(PEG). (C) Interpenetration of the polymers at the PEG/PVA interface. The blue and red atoms indicate the PEG and PVA chains, respectively.

■ CONCLUSION

We have reported the surface functionalization of the outer surface of ZIF-8 NPs of 25 nm in diameter with PEG of two chain lengths (480 Da and 5000 Da) through the Graftfast method. This protocol has led to a selective and covalent surface modification of ZIF-8 NPs following a rapid reaction at RT and in water. PEG brushes were grafted onto the surface of ZIF-8 NPs without significant blocking of the MOF internal porosity and preserving its crystallinity. More importantly, the PEG shell significantly enhances the chemical stability of ZIF-8 NPs in water. Due to the efficient shielding of PEG-g-ZIF-8 NPs by the PEG corona, colloidal solutions with a remarkable stability over time could be prepared and were used to cast defect-free CL-PEG$_{5000}$-g-ZIF-8/PVA MMMs with a MOF content of 15 wt%. Finally, supported CL-PEG$_{5000}$-g-ZIF-8/PVA based

MMMs were prepared with enhanced transport properties for the dehydration of IPA by pervaporation. This was mainly attributed to a synergism effect related to the co-reticulation of the membrane by GA and PEG_{5000}-g-ZIF-8 NPs. The absence of interfacial defects of the membranes and the high compatibility between PEGylated ZIF-8 NPs and PVA can be explained at the molecular level by the interpenetration of PVA/PEG polymer chains and the existence of strong site-site interactions between them, as proved by molecular modelling. Furthermore, the simulations also suggest a higher contact surface between PVA and PEG chains than that between the PVA chains and the MOF.

■ ASSOCIATED CONTENT

Supporting Information. Protocol for the synthesis of ZIF-8 NPs. Methods for the characterization of PEGylated ZIF-8 NPs. SEM/TEM images and SAXS curves of PEGylated and non-modified ZIF-8 NPs. Evaluation of the PEG density at the surface of ZIF-8. Colloidal stability of PEGylated and non-modified ZIF-8 NPs upon ageing. Characterizations of PEG-g-ZIF-8/PVA membranes. Details of the simulations of ZIF-8/PVA and PEG/PVA interfaces. This information is available free of charge via the Internet at http://pubs.acs.org/.

■ AUTHOR INFORMATION

Corresponding author

christian.serre@ens.fr; Guillaume.Maurin@univ-montp2.fr; nathalie.steunou@uvsq.fr;

REFERENCES

(1) Themed issue, *Chem. Soc. Rev.* **2017**,*46*, 3104-3481.

(2) Cepeda, J.;Perez-Yanez, S.; Beobide, G. ;Castillo, O.; Goikolea, E.; Aguesse, F.; Garrido, L.; Luque, A.; Wright, P. A. Scandium/Alkaline Metal-Organic Frameworks: Adsorptive Properties and Ionic Conductivity. *Chem. Mater.* **2016**, *28*, 2519−2528, DOI 10.1021/acs.chemmater.5b03458.

(3) Yang, Q.; Vaesen, S.; Ragon, F.; Wiersum, A. D.; Wu, D.; Lago, A.; Devic, T.; Martineau, C.; Taulelle, F.; Llewellyn, P. L.; Jobic, H.; Zhong, C.; Serre, C.; De Weireld, G.; Maurin, G. A Water Stable Metal–Organic Framework with Optimal Features for CO_2 Capture. *Angew. Chem. Int. Ed.* **2013**, *52*, 10316–10320, DOI 10.1002/anie.201302682.

(4) Hu, Z.; Nalaparaju, A.; Peng, Y.; Jiang, J.; Zhao, D. Modulated Hydrothermal Synthesis of UiO-66(Hf)-Type Metal−Organic Frameworks for Optimal Carbon Dioxide Separation. *Inorg. Chem.* **2016**, *55*, 1134−1141, DOI 10.1021/acs.inorgchem.5b02312.

(5) Wang, Z.; Cohen, S. M. Postsynthetic Modification of Metal–Organic Frameworks. *Chem. Soc. Rev*. **2009**, *38*, 1315–1329, DOI 10.1039/b802258p.

(6) Von Zons, T.; Brokmann, L.; Lippke, J.; Preuße, T.; Hülsmann, M.; Schaate, A.; Behrens, P.; Godt, A. Postsynthetic Modification of Metal–Organic Frameworks through Nitrile Oxide–Alkyne Cycloaddition. *Inorg. Chem.* **2018**, *57*, 3348–3359, DOI 10.1021/acs.inorgchem.8b00126.

(7) Kaneti, Y. V.; Dutta, S.; Hossain, M. S. A.; Shiddiky, M. J. A.; Tung, K. –L.; Shieh, F. –K.; Tsung, C. –K.; Wu, K. C. W.; Yamauchi, Y. Strategies for Improving the Functionality of Zeolitic Imidazolate Frameworks: Tailoring Nanoarchitectures for Functional Applications. *Adv. Mater.* **2017**, *29*, 1700213. DOI 10.1002/adma.201700213.

(8) Bellido, E.; Hidalgo, T.; Lozano, M. V.; Guillevic, M.; Simón-Vázquez, R.; Santander-Ortega, M. J.; González-Fernández, Á.; Serre, C.; Alonso, M. J.; Horcajada, P. Heparin-Engineered Mesoporous Iron Metal-Organic Framework Nanoparticles: Toward Stealth Drug Nanocarriers. *Adv. Healthcare. Mater.* **2015**, *4*, 1246–1257, DOI 10.1002/adhm.201400755.

(9) Hidalgo Crespo, T.; Giménez-Marqués, M.; Bellido, E.; Ávila, J.; Asensio, M.; Salles, F.; Lozano, M.; Guillevic, M.; Simón-Vázquez, R.; González-Fernández, A.; Serre, C.; Alonso, M. J.; Horcajada, P. Chitosan-Coated Mesoporous MIL-100(Fe) Nanoparticles as Improved Bio-Compatible Oral Nanocarriers. *Sci. Rep.* **2017**, *7*, 43099, DOI 10.1038/srep43099.

(10) Rijnaarts, T.; Mejia-Ariza, R.; Egberink, R. J. M.; van Roosmalen, W.; Huskens, J. Metal–Organic Frameworks (MOFs) as Multivalent Materials: Size Control and Surface Functionalization by Monovalent Capping Ligands. *Chem. Eur. J.* **2015**, *21*, 10296 – 10301, DOI 10.1002/chem.201501974

(11) Mejia-Ariza, R.; Huskens, J. The effect of PEG length on the size and guest uptake of PEG-capped MIL-88A particles. *J. Mater. Chem. B.* **2016**, *4*, 1108-1115, DOI 10.1039/c5tb01949d.

(12) Nagata, S.; Kokado, K.; Sada, K. Metal-Organic Framework Tethering PNIPAM For ON-OFF Controlled Release in Solution. *Chem. Commun.* **2015**, *51*, 8614-8617, DOI 10.1039/c5cc02339d.

(13) Seoane, B.; Coronas, J.; Gascon, I.; Benavides, M. E.; Karvan, O.; Caro, J.; Kapteijn, F.; Gascon, J. Metal–Organic Framework based Mixed Matrix Membranes: a Solution for Highly Efficient CO_2 Capture? *Chem. Soc. Rev.* **2015**, *44*, 2421-2454, DOI 10.1039/c4cs00437j.

(14) Denny, Jr., M. S.; Moreton, J. C.; Benz, L.; Cohen, S. M. Metal-organic Frameworks for Membrane-based Separations. *Nature Rev. Mater.* **2016**, 16078, DOI 10.1038/natrevmats2016.78.

(15) Benzaqui, M.; Pillai, R. S.; Sabetghadam, A.; Benoit, V.; Normand, P.; Marrot, J.; Menguy, N.; Montero, D.; Shepard, W.; Tissot, A.; Martineau-Corcos, C.; Sicard, C.; Mihaylov, M.; Carn, F.; Beurroies, I.; Llewellyn, P. L.; De Weireld, G.; Hadjiivanov, K.; Gascon, J.; Kapteijn, F.; Maurin, G.; Steunou, N.; Serre, C. Revisiting the Aluminum Trimesate-Based MOF (MIL-96): From Structure Determination to the Processing of Mixed Matrix Membranes for CO_2 Capture. *Chem. Mater.* **2017**, *29*, 10326−10338, DOI 10.1021/acs.chemmater.7b03203.

(16) Sabetghadam, A.; Liu, X.; Benzaqui, M. ; Gkaniatsou, E.; Orsi, A.; Lozinska, M. M.; Sicard, C.; Johnson, T.; Steunou, N.; Wright, P. A.; Serre, C.; Gascon, J.; Kapteijn, F. Influence of Filler Pore Structure and Polymer on the Performance of MOF-based Mixed Matrix Membranes for CO2 Capture. *Chem. Eur. J.* **2018**, *24*, 7949 -7956, DOI 10.1002/chem.201800253.

(17) Liu, G.; Chernikova, V.; Liu, Y.; Zhang, K.; Belmabkhout, Y.; Shekhah, O.; Zhang, C.; Yi, S.; Eddaoudi, M.; Koros, W. J. Mixed Matrix Formulations with MOF Molecular Sieving for Key Energy-Intensive Separations. *Nature Mater.* **2018**, *17*, 283-289, DOI 10.1038/s41563-017-0013-1.

(18) Zimpel, A.; Preiß, T.; Röder, R.; Engelke, H.; Ingrisch, M.; Peller, M.; Rädler, J. O.; Wagner, E.; Bein, T.; Lächelt, U.; Wuttke, S. Imparting Functionality to MOF Nanoparticles by External Surface Selective Covalent Attachment of Polymers. *Chem. Mater.* **2016**, *28*, 3318–3326, DOI 10.1021/acs.chemmater.6b00180.

(19) Wang, S.; Morris, W.; Liu, Y.; McGuirk, C. M.; Zhou, Y.; Hupp, J. T.; Farha O. K.; Mirkin, C. A. Surface-Specific Functionalization of Nanoscale Metal–Organic Frameworks. *Angew. Chem. Int. Ed.* **2015**, *54*, 14738 –14742. DOI 10.1002/anie.201506888.

(20) Agostoni, V.; Horcajada, P.; Noiray, M.; Malanga, M.; Aykaç, A.; Jicsinszky, L.; Vargas-Berenguel, A.; Semiramoth, N.; Daoud-Mahammed, S.; Nicolas, V.; Martineau, C.; Taulelle, F.; Vigneron, J.; Etcheberry, A.; Serre, C.; Gref, R. A. ''Green'' Strategy to Construct Non-covalent, Stable and Bioactive Coatings on Porous MOF Nanoparticles. *Sci. Rep.* **2015**, *5*, 7925, DOI 10.1038/srep07925.

(21) Wang, S.; McGuirk, C. M.; Ross, M. B.; Wang, S.; Chen, P.; Xing, H.; Liu, Y.; Mirkin, C. A. General and Direct Method for Preparing Oligonucleotide-Functionalized Metal−Organic Framework Nanoparticles. *J. Am. Chem. Soc.* **2017**, *139*, 9827−9830, DOI: 10.1021/jacs.7b05633.

(22) He, C.; Lu, K.; Liu, D.; Lin, W. Nanoscale Metal−Organic Frameworks for the Co-Delivery of Cisplatin and Pooled siRNAs to Enhance Therapeutic Efficacy in Drug-Resistant Ovarian Cancer Cells. *J. Am. Chem. Soc.* **2014**, *136*, 5181−5184, DOI 10.1021/ja4098862.

(23) Jung, S.; Kim, Y.; Kim, S.-J.; Kwon, T.-H.; Huh, S.; Park, S. Biofunctionalization of Metal-Organic Frameworks by Covalent Protein Conjugation. *Chem. Commun.* **2011**, *47*, 2904−2906, DOI 10.1039/C0CC03288C.

(24) He, C.; Lu, K.; Lin, W. Nanoscale Metal−Organic Frameworks for Real-Time Intracellular pH Sensing in Live Cells. *J. Am. Chem. Soc.* **2014**, *136*, 12253−12256, DOI 10.1021/ja507333c.

(25) Abánades Lázaro, I.; Haddad, S.; Sacca, S.; Orellana-Tavra, C.; Fairen-Jimenez, D.; Forgan, R. S. Selective Surface PEGylation of UiO-66 Nanoparticles for Enhanced Stability, Cell Uptake, and pH-Responsive Drug Delivery. *Chem* **2017**, *2* (4), 561–578, DOI 10.1016/j.chempr.2017.02.005.

(26) McDonald, K. A.; Feldblyum, J.; Koh, K.; Wong-Foy, A. G.; Matzger, A. J. Polymer@MOF@MOF: ″Grafting From″ Atom Transfer Radical Polymerization for the Synthesis of Hybrid Porous Solids. *Chem. Commun.* **2015**, *51*, 11994−11996, DOI 10.1039/c5cc03027g.

(27) Xie, K.; Fu, Q.; He, Y.; Kim, J.; Goh, S. J.; Nam, E.; Qiao, G. G.; Webley, P. A. Synthesis of Well Dispersed Polymer Grafted Metal–Organic Framework Nanoparticles. *Chem. Commun.,* **2015**, *51*, 15566-15569, DOI 10.1039/c5cc06694h.

(28) Hou, L.; Wang, L.; Zhang, N.; Xie, Z.; Dong, D. Polymer Brushes on Metal–Organic Frameworks by UV-induced Photopolymerization. *Polym. Chem.* **2016**, *7*, 5828–5834, DOI 10.1039/c6py01008c.

(29) Mc Guire, C. V.; Forgan, R. S. The Surface Chemistry of Metal–Organic Frameworks. *Chem. Commun.* **2015**, *51*, 5199-5217, DOI 10.1039/c4cc04458d.

(30) Semino R.; Ramsahye, N. A.; Ghoufi, A.; Maurin G. Microscopic Model of the Metal-Organic Framework/Polymer Interface: A First Step toward Understanding the Compatibility in Mixed Matrix Membranes. *ACS Appl. Mater. Interfaces* **2016,** *8,* 809-819, DOI 10.1021/acsami.5b10150.

(31) Benzaqui, M.; Semino, R.; Menguy, N.; Carn, F.; Kundu, T.; Guigner, J.-M.; McKeown, N. B.; Msayib, K. J.; Carta, M.; Malpass-Evans, R.; Le Guillouzer, C.; Clet, G.; Ramsahye, N. A.; Serre, C.; Maurin, G.; Steunou, N. Toward an Understanding of the Microstructure and Interfacial Properties of PIMs/ZIF-8 Mixed Matrix Membranes. *ACS Appl. Mater. Interfaces* **2016**, *8*, 27311–27321, DOI 10.1021/acsami.6b08954.

(32) Semino, R.; Moreton, J. C.; Ramsahye, N. A.; Cohen, S. M.; Maurin, G. Understanding the Origins of Metal-Organic Framework/Polymer Compatibility. *Chem. Sci.* **2018**, *9*, 315–324, DOI 10.1039/c7sc04152g.

(33) Mesnage, A.; Lefevre, X.; Jegou, P.; Deniau, G.; Palacin, S. Spontaneous Grafting of Diazonium Salts: Chemical Mechanism on Metallic Surfaces. *Langmuir* **2012**, *28,* 11767−11778, DOI 10.1021/la3011103.

(34) Mesnage, A.; Esnouf, S.; Jegou, P.; Deniau, G.; Palacin, S. Understanding the Redox-Induced Polymer Grafting Process: A Dual Surface-Solution Analysis. *Chem. Mater.* **2010**, *22*, 6229–6239, DOI 10.1021/cm1014702.

(35) Banerjee, R.; Phan, A.; Wang, B.; Knobler, C.; Furukawa, H.; O'Keeffe, M.; Yaghi, O. M. High-Throughput Synthesis of Zeolitic Imidazolate Frameworks and Application to CO_2 Capture. *Science* **2008**, *319*, 939-943. DOI 10.1126/science.1152516

(36) Liang, W.; Ricco, R.; Maddigan, N. K.; Dickinson, R. P.; Xu, H.; Li, Q.; Sumby, C. J.; Bell, S. G.; Falcaro, P.; Doonan, C. J. Control of Structure Topology and Spatial Distribution of Biomacromolecules in Protein@ZIF-8 Biocomposites. *Chem. Mater.* **2018**, 30, 1069-1077, DOI 10.1021/acs.chemmater.7b04977.

(37) Dai, Y.; Johnson, J. R.; Karvan, O.; Sholl, D. S. ; Koros, W. J. Ultem®/ZIF-8 Mixed Matrix Hollow Fiber Membranes for CO_2/N_2 Separations. *J. Membr. Sci.* **2012**, *401-402*, 76-82, DOI 10.1016/j.memsci.2012.01.044.

(38) Shekhah, O.; Swaidan, R.; Belmabkhout, Y.; du Plessis, M.; Jacobs, T.; Barbour, L. J.; Pinnau, I.; Eddaoudi, M. The Liquid Phase Epitaxy Approach for the Successful Construction of Ultra-thin and Defect-free ZIF-8 Membranes: Pure and Mixed Gas Transport Study. *Chem. Commun.* **2014**, *50*, 2089-2092, DOI 10.1039/C3CC47495J.

(39) Deng, Y.–H.; Chen, J. -T.; Chang, C. –H.; Liao, K.-S.; Tung, K. –L.; Price, W. E.; Yamauchi, Y.; Wu, K. C. W. Drying-Free, Water-Based Process for Fabricating Mixed-Matrix Membranes with Outstanding Pervaporation Performance. *Angew. Chem. Int. Ed.* **2016**, *55*, 12793 –12796, DOI 10.1002/anie.201607014.

(40) Liu, X.; Li, Y.; Ban, Y.; Peng, Y.; Jin, H.; Bux, H.; Xu, L.; Caro, J.; Yang, W. Improvement of Hydrothermal Stability of Zeolitic Imidazolate Frameworks. *Chem. Commun.* **2013**, *49*, 9140-9142, DOI: 10.1039/c3cc45308a.

(41) Zhang, H. ; James, J.; Zhao, M.; Yao, Y.; Zhang, Y.; Zhang, B.; Lin, Y. S. Improving Hydrostability of ZIF-8 Membranes via Surface Ligand Exchange. *J. Membr. Sci.* **2017**, *532*, 1-8, DOI 10.1016/j.memsci.2017.01.065.

(42) Zhang, H.; Liu, D.; Yao, Y.; Zhang, B.; Lin, Y. S. Stability of ZIF-8 Membranes and Crystalline Powders in Water at Room Temperature, *J. Membr. Sci.* **2015**, *485*, 103–111, DOI 10.1016/j.memsci.2015.03.023.

(43) Wang, H.; Jian, M.; Qi, Z.; Li, Y.; Liu, R.; Qu, J. Specific Anion Effects on the Stability of Zeolitic Imidazolate Framework-8 in Aqueous Solution. *Microporous Mesoporous Mater.* **2018**, *259*, 171-177, DOI 10.1016/j.micromeso.2017.10.011.

(44) Yin, H.; Kim, H.; Choi, J.; Yip, A.C.K. Thermal Stability of ZIF-8 Under Oxidative and Inert Environments: a Practical Perspective on Using ZIF-8 as a Catalyst Support, *Chem. Eng. J.* **2015**, *278*, 293–300, DOI 10.1016/j.cej.2014.08.075.

(45) Tsai, C.-W.; Langner, E. H. G. The Effect of Synthesis Temperature on the Particle Size of Nano-ZIF-8. *Microporous Mesoporous Mater.* **2016**, *221*, 8–13, DOI 10.1016/j.micromeso.2015.08.041.

(46) Cravillon, J.; Münzer, S.; Lohmeier, S.-J.; Feldhoff, A.; Huber, K.; Wiebcke, M. Rapid Room-Temperature Synthesis and Characterization of Nanocrystals of a Prototypical Zeolitic Imidazolate Framework. *Chem. Mater.* **2009**, *21*, 1410–1412. DOI 10.1021/cm900166h

(47) Allen, C.; Dos Santos, N.; Gallagher, R. ; Chiu, G. N. C. ; Shu, Y. ; Li, W. M. ; Johnstone, S. A. ; Janoff, A. S.; Mayer, L. D.; Webb, M. S. Bally, M. B. Controlling the Physical Behavior and Biological Performance of Liposome Formulations through Use of Surface Grafted Poly(ethylene Glycol). *Biosc. Rep.* **2002**, *22*, 225-250.

(48) Berthelot, T.; Bellido Vera, E.; Gref, R.; Horcajada Cortes, P.; Serre, C.; Couvreur, P. Porous Solid with Outer Surface Grafted with a Polymer. European Patent, EP14188166   October 8th, 2014.

(49) Giménez-Marqués, M.; Bellido, E.; Berthelot, T.; Simón-Yarza, T.; Hidalgo, T.; Avila, J.; Asensio, M. C.; Simón-Vázquez, R.; González-Fernández, A.; Gref, R.; Couvreur, P.; Serre, C.; Horcajada, P. Graftfast surface modification of MOFs: improving nanocarrier therapeutic efficacy. *Small* **2018**, *14*, 1801900, DOI 10.1002/smll.201801900.

(50) Wuelfing, W. P.; Gross, S. M.; Miles, D. T.; Murray, R. W. Nanometer Gold Clusters Protected by Surface-Bound Monolayers of Thiolated Poly(ethylene Glycol) Polymer Electrolyte. *J. Am. Chem. Soc.* **1998**, *120*, 12696–12697, DOI 10.1021/ja983183m.

(51) Sebby, K. B.; Mansfield, E. Determination of the Surface Density of Polyethylene Glycol on Gold Nanoparticles by Use of Microscale Thermogravimetric Analysis. *Anal. Bioanal. Chem.* **2015**, *407*, 2913–2922, DOI 10.1007/s00216-015-8520-x.

(52) Auguste, D. T.; Armes, S. P.; Brzezinska, K. R.; Deming, T. J.; Kohn, J.; Prud'homme, R. K. pH Triggered Release of Protective Poly(Ethylene Glycol)-b-Polycation Copolymers from Liposomes. *Biomaterials* **2006**, *27*, 2599–2608, DOI 10.1016/j.biomaterials.2005.08.036.

(53) Xu, Q.; Ensign, L. M.; Boylan, N. J.; Schön, A.; Gong, X.; Yang, J. –C.; Lamb, N. W.; Cai, S.; Freire, E.; Hanes, J. Impact of Surface Polyethylene Glycol (PEG) Density on Biodegradable Nanoparticle Transport in Mucus ex Vivo and Distribution in Vivo. *ACS Nano* **2015**, *9*, 9217-9227, 10.1021/acsnano.5b03876.

(54) F. –L. Li, H. –X. Li, J.-P. Lang, Fabrication of Yolk–Shell Pd@ZIF-8 Nanoparticles With Excellent Catalytic Size-selectivity For The Hydrogenation of Olefins. *CrystEngComm.* **2016**, *18*, 1760-1767, DOI 10.1039/C5CE02219C.

(55) Ojha, S.; Dang, A.; Hui, C. M.; Mahoney, C.; Matyjaszewski, K. ; Bockstaller, M. R. Strategies for the Synthesis of Thermoplastic Polymer Nanocomposite Materials with High Inorganic Filling Fraction. *Langmuir* **2013**, *29*, 8989−8996, DOI org/10.1021/la401522v.

(56) Borukhov, I.; Leibler, L. Enthalpic Stabilization of Brush-Coated Particles in a Polymer Melt. *Macromolecules* **2002**, *35*, 5171−5182, DOI 10.1021/ma011351g.

(57) Sawamura, K-I.; Furuhata, T.; Sekine,Y.; Kikuchi, E.; Subramanian, B.; Matsukata, M. Zeolite Membrane for Dehydration of Isopropylalcohol-Water Mixture by Vapor Permeation. *ACS Appl. Mater. Interfaces* **2015**, *7*, 13728−13730, DOI: 10.1021/acsami.5b04085.

(58) Dmitrenko, M.; Penkova, A.; Kuzminova, A.; Missyul, A.; Ermakov, S.; Roizard, D. Development and Characterization of New Pervaporation PVA Membranes for the Dehydration using Bulk and Surface Modifications. *Polymer* **2018**, *10*, 571, DOI 10.3390/polym10060571.

(59) Cheng, P.-I.; Hong, P.-D.; Lee, K.-R.; Lai, J. -Y.; Tsai, Y.-L. High Permselectivity of Networked PVA/GA/Cs-Ag$^+$- Membrane for Dehydration of Isopropanol. *J. Membr. Sci.* **2018**, *564*, 926–934, DOI 10.1016/j.memsci.2018.06.019.

(60) Assender, H. E.; Windle, A. H. Crystallinity in Poly(vinyl alcohol).1. An X-ray Diffraction Study of Atactic PVOH. *Polymer* **1998**, 39, 4295-4302.

(61) Penkova, A. V.; Acquah, S. F. A.; Sokolova, M. P.; Dmitrenko, M. E.; Toikka, A. M. Polyvinylalcohol Membranes Modified by Low-hydroxylated Fullerenol $C_{60}(OH)_{12}$. *J. Membr. Sci.* **2015**, *491*, 22–27, DOI 10.1016/j.memsci.2015.05.011.

(62) Ravindra, S.; Rajinikanth, V.; Mulaba-Bafubiandi, A. F. ; Vallabhapurapu, V. S. Performance Enhancement of the Poly (vinyl alcohol) (PVA) by Activated Natural Clay Clinoptilolite for Pervaporation Separation of Aqueous–Organic Mixtures. *Desalin. Water Treat.* **2015**, *57*, 4920-4934, DOI 10.1080/19443994.2014.999131.

(63) Amirilargani, M. ; Ahmadzadeh Tofighy, M. ; Mohammadi, T.; Sadatnia, B. Novel Poly(vinyl alcohol)/Multiwalled Carbon Nanotube Nanocomposite Membranes for Pervaporation Dehydration of Isopropanol: Poly(sodium 4-styrenesulfonate) as a Functionalization Agent. *Ind. Eng. Chem. Res.* **2014**, *53*, 12819−12829, DOI 10.1021/ie501929m.

(64) Amirilargani, M.; Sadatnia, B.; Poly(vinyl alcohol)/zeolitic Imidazolate Frameworks (ZIF-8) Mixed Matrix Membranes for Pervaporation Dehydration of Isopropanol. *J. Membr. Sci.* **2014**, *469*, 1–10, DOI 10.1016/j.memsci.2014.06.034.

(65) Semino, R.; Dürholt, J. P.; Schmid, R.; Maurin, G. Multiscale Modeling of the HKUST-1/Poly(vinyl alcohol) Interface: From an Atomistic to a Coarse Graining Approach. *J. Phys. Chem. C* **2017**, *121*, 21491-21496, DOI 10.1021/acs.jpcc.7b07090